

# The Muon-Induced Neutron Indirect Detection EXperiment, MINIDEX

I. Abt<sup>a</sup>, A. Caldwell<sup>a</sup>, C. Carissimo<sup>a</sup>, C. Gooch<sup>a</sup>, R. Kneißl<sup>a</sup>, J. Langford<sup>a</sup>,  
X. Liu<sup>a</sup>, B. Majorovits<sup>a</sup>, M. Palermo<sup>a,\*</sup>, O. Schulz<sup>a</sup>, L. Vanhoefer<sup>a</sup>

<sup>a</sup>*Max-Planck-Institut für Physik, Munich, Germany*

---

## Abstract

A new experiment to quantitatively measure neutrons induced by cosmic-ray muons in selected high-Z materials is introduced. The design of the Muon-Induced Neutron Indirect Detection EXperiment, MINIDEX, and the results from its first data taking period are presented as well as future plans. Neutron production in high-Z materials is of particular interest as such materials are used for shielding in low-background experiments. The design of next-generation large-scale experiments searching for neutrinoless double beta decay or direct interactions of dark matter requires reliable Monte Carlo simulations of background induced by muon interactions. The first five months of operation already provided a valuable data set on neutron production and neutron transport in lead. A first round of comparisons between MINIDEX data and Monte Carlo predictions obtained with two GEANT4-based packages is presented. The rate of muon-induced events is overall a factor three to four higher in data than predicted by the Monte Carlo packages. In addition, the time evolution of the muon-induced signal is not well described by the simulations.

*Keywords:* muon-induced neutrons, low-background experiments, Monte Carlo simulation

---

## 1. Introduction

Muon-induced neutrons are not only an interesting physics topic by themselves, but they are also a potentially very important source of background in searches for new rare phenomena like neutrinoless double beta decay or directly observable interactions of dark matter.

---

\*Corresponding Author. Tel: +49-89-32354295  
*Email address:* palermo@mpp.mpg.de (M. Palermo)

The Muon-Induced Neutron Indirect Detection EXperiment (MINIDEX) was designed to provide data on the interactions of cosmic high-energy muons in high-Z materials. Previous measurements are not really consistent [1, 2, 3, 4, 5, 6, 7]. Neither are the corresponding calculations [8, 9, 10, 1, 11]. One of the problems is, that for all measurements, it is hard to disentangle the primary neutron production rate from the influence of neutron transport. In addition, experiments have different energy thresholds for the detection of neutrons. MINIDEX detects thermalised neutrons and thus, has no neutron-energy threshold. Another problem is the determination of the background. MINIDEX measures its own background to high precision simultaneously with the signal.

Neutrons produced by the interactions of high-energy muons with nuclei are emitted in all directions and have energies of up to several GeV. As their energy exceeds the maximum energy of neutrons produced by natural radioactivity by several orders of magnitude, they can be important for low-background experiments, even though they are much more rare [12, 13, 14, 15, 16]. The importance of muon-induced background will increase for the next generation of low-background experiments, because the background level will have to be reduced by at least another order of magnitude compared to currently running experiments [17, 18, 19, 20].

Traditionally, high-Z materials are used to shield low-background experiments. Examples are the MAJORANA [21] and CDEX I [22] projects. However, in such a configuration, muons produce high-energy neutrons in the shield, close to the active volume. Therefore, besides going deeper underground, techniques to veto muons are commonly used. However, moderated neutrons can create unstable states close to or in the active volume of an experiment which decay too slowly to be vetoed against. A lot of effort went into Monte Carlo packages [12, 23, 24, 25, 26] to facilitate the evaluation of such backgrounds. Nevertheless, all Monte Carlo predictions depend on the input assumptions about the primary neutron-production processes, neutron transport and neutron thermalisation. As a result, the predictions vary substantially for the different packages [27, 12, 13, 16, 28, 29, 30, 31, 32, 15]; summaries and discussions in [33, 34, 35].

The data accumulated with MINIDEX provide information on muon-induced neutron production and transport by detecting thermalised neutrons. For its first runs, MINIDEX was operated using lead as the target material. However, it was designed to provide data sets for a number of selected high-Z materials. The first data, taken from July 15 to November 25, 2015, are presented as well a comparison with GEANT-based Monte Carlo predictions.

## 2. The experimental setup

MINIDEX was designed such that it can be operated remotely. It is compact to fit into relatively small facilities, can be moved easily and the target material can be exchanged. It has to be operated underground to suppress background from cosmogenic neutrons. As the experiment is relatively small, shallow sites are required to have a large enough muon flux to obtain reasonable data rates. MINIDEX was installed for its first data taking period, run I, in the Tübingen Shallow Underground Laboratory (TSUL) in July, 2015. The nominal overburden of the TSUL corresponds to  $\approx 16$  meter water equivalent [36].

The detection strategy, see also Fig. 1, is:

- muons passing through the high- $Z$  material are tagged with plastic scintillator panels;
- they interact with the high- $Z$  target material;
- the muon-induced neutrons emerging from the high- $Z$  volume are thermalised in water and eventually captured by hydrogen nuclei;
- the 2.2 MeV gammas emitted after the neutron capture are identified by germanium detectors;
- the signal is 2.2 MeV gammas recorded within a predefined time window after the passage of a muon;
- the background is measured between the end of the signal window and the passage of the next muon.

An important feature is that the background is measured by MINIDEX itself without the need of any Monte Carlo calculation.

Indirect neutron detection through thermal capture in a selected isotope with subsequent gamma ray emission is a standard technique to detect neutrons [30, 34]. The plastic scintillator panels tagging the muons work independently from the germanium detectors identifying neutron captures. Thus, there are no inefficiencies due to time resolution, which can be a problem for experiments using the same detectors to identify muons and neutrons.

Lead was chosen as the target material for run I as it is one of the most commonly used materials for high- $Z$  shielding in deep underground experiments [30, 21, 18, 22].

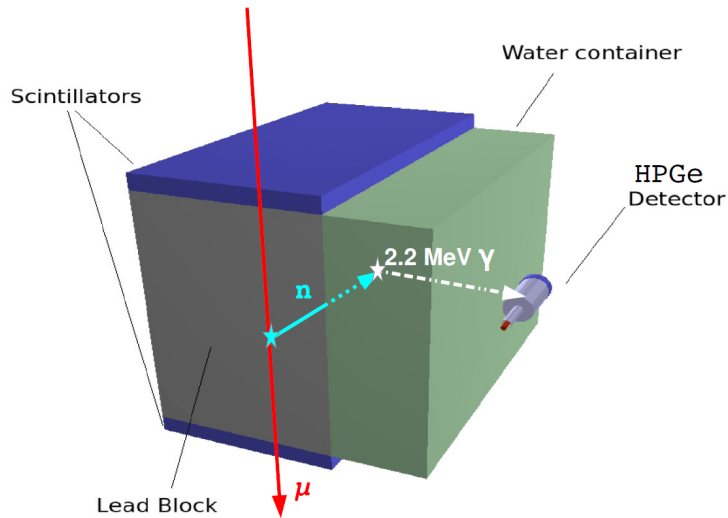


Figure 1: Muon-induced neutrons are observed indirectly through capture in water with subsequent gamma ray emission. Scintillators are used for muon tagging. From [35].

### 2.1. Run I geometry

MINIDEX is a compact apparatus with a foot-print of  $65 \times 75 \text{ cm}^2$  and a height of 60.5 cm. It consists of a lead castle with outer dimensions of  $65 \times 75 \times 50.5 \text{ cm}^3$ . Plastic scintillator panels, 5 cm thick, exactly cover the lead surfaces at the top and the bottom of the setup. The outer view of the MINIDEX apparatus is depicted in Fig. 2(a).

A rectangular container with outer dimensions  $35 \times 55 \times 30 \text{ cm}^3$ , filled with ultra-pure water, is located inside the lead castle as shown in Figs. 2(b) and 3. This container is made of plastic ( $\text{C}_{10}\text{H}_8\text{O}_4$ ) and has a wall-thickness of 1 cm. The minimum thickness of the water layer of about 9 cm was optimized such that the probability to capture a neutron entering the water volume is about 95 % [35].

The water container has a central hole which runs through the whole length of the container. It is 13 cm wide and 8 cm high. Two high-purity germanium (HPGe) detectors are placed in this hole, facing the center of the water container.

As a support for the top layer of lead, there is a 0.5 cm thick copper plate, see Fig. 4(d). This copper plate avoids any weight load on the water container. Copper was chosen due to its relative low weight compared to its strength.

Photos of the MINIDEX setup during construction are shown in Fig. 4.

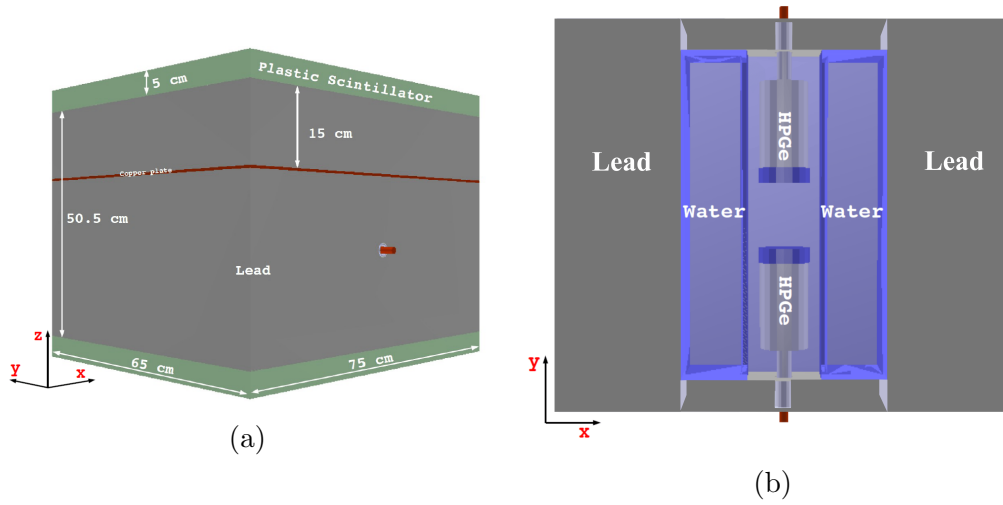


Figure 2: Schematic (a) of the outside of MINIDEX, (b) central cut from the top of MINIDEX. Both adapted from [35].

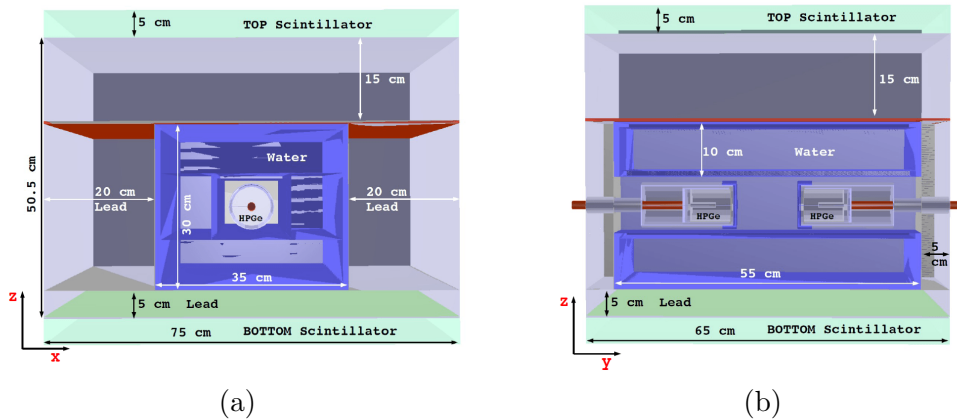


Figure 3: Schematic of central cuts through MINIDEX: (a) from the front, (b) from the side. Both adapted from [35].

The lead castle is placed on top of a heavy-load table (surface area of  $100 \times 150 \text{ cm}^2$ ) with aluminum framing as shown in Fig. 5. The bottom scintillator, supported by an aluminum structure, is placed underneath the table top; this is not indicated in Figs. 2 and 3. The lower shelf of the table is used for the data acquisition (DAQ) system and all electronic devices needed to operate MINIDEX. The complete MINIDEX run I setup is shown in Fig. 5. It was installed in the Tübingen Shallow Underground Laboratory in less than three days.

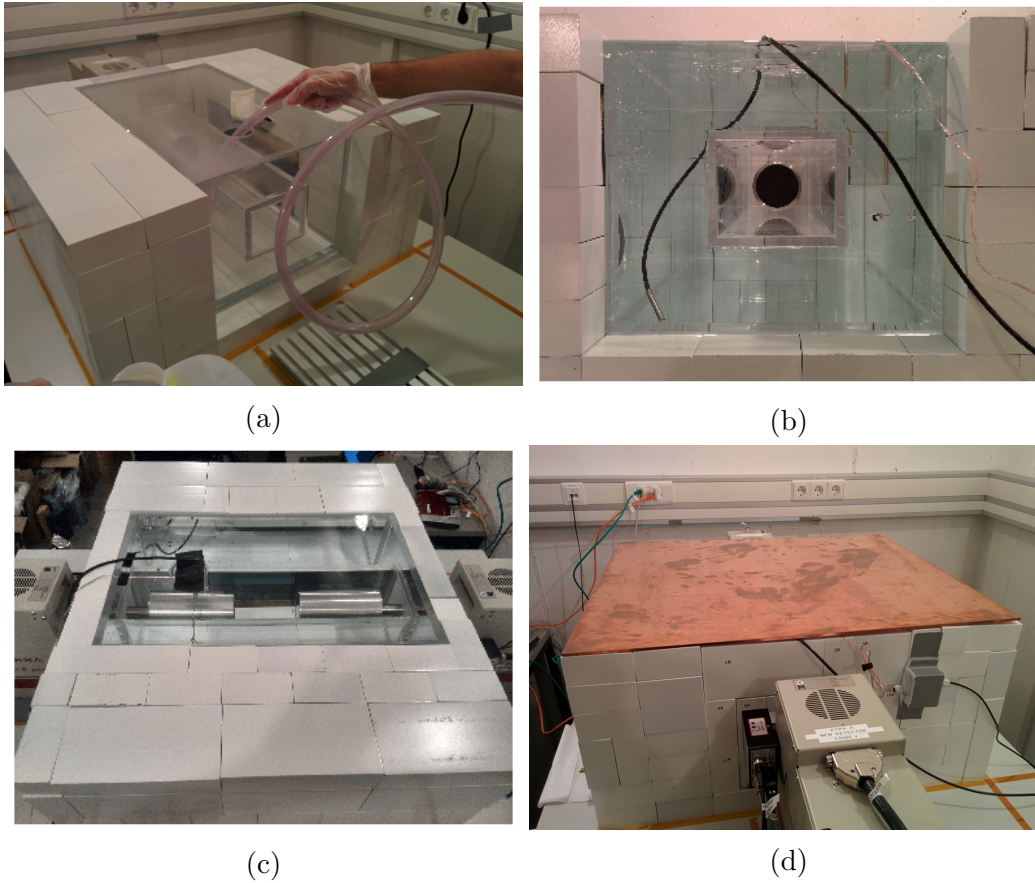


Figure 4: (a) Partially built up lead castle with water tank being filled; (b) frontal view into MINIDEX with one germanium detector inserted from the other side; (c) view from the open top onto the two germanium detectors; (d) the setup covered by the structural copper plate before stacking the lead on top.

## 2.2. Physics composition of signal and background

The signal for run I was defined as 2.2 MeV gamma events recorded in a predefined time window after the passage of a muon through the top and bottom scintillators. Muons going vertically through a side-wall had energies of at least 1.2 GeV; muons passing diagonally could have substantially lower energies. Events were counted as signal independently of the location of the muon interaction, which could not be determined in the run I geometry. Some small number of events were counted as signal even though a muon only passed one scintillator panel, because a secondary particle deposited energy in the bottom scintillator.

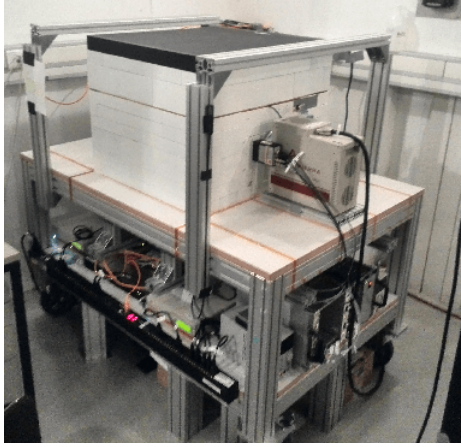


Figure 5: The MINIDEX run I setup completely installed in the Tübingen Shallow Underground Laboratory. Visible are the lead castle, the top scintillator panel, the electrical cooling unit of one of the germanium detectors and some electronic equipment on the lower shelf of the table.

Background are events with a 2.2 MeV gamma recorded due to

- neutrons induced by non-triggering muons;
  - passing close by, but not entering the setup;
  - passing only one of the scintillator panels due to geometrical reasons;
  - being stopped in the apparatus;
- cosmogenic neutrons;
  - due to the remnant cosmic neutron flux within TSUL;
- neutrons from natural radioactivity;
  - from fission;
  - from  $(\alpha, n)$ -reactions.

### 2.3. Detectors

The MINIDEX run I setup requires only four detectors to be read out: two plastic scintillator panels and two HPGe detectors.

The two scintillator panels for run I, produced by Saint-Gobain Crystals [37], were made of BC-408 (Polyvinyltoluene,  $C_{10}H_{11}$ ) with a density of

1.032 g/cm<sup>3</sup>. The wavelength of maximum emission was  $\approx 425$  nm. Both the photomultiplier tubes (PMT) and the PMT HV bases (model HV2520AN) were embedded inside the panel volumes and no wavelength shifters were used to collect the light of the scintillators onto the PMT photocathodes. The PMTs had a diameter of 30 mm and were produced by ET Enterprises [38](model 9900B). The active diameter was 25 mm and the spectral range was 280 nm to 680 nm, with a peak quantum efficiency of 26 % at around 400 nm. Sensitive PMT sidewalls allowed for wide-angle light detection. The tube housing the multiplication dynodes was  $\approx 9$  cm long.

The novel approach of having the PMTs incorporated in the scintillator panels was chosen as it is particularly space saving. However, the panels proved to be not fully efficient over the whole surface area. The top and bottom panels were efficient to  $86.53 \pm 0.10$  and  $92.69 \pm 0.15$  %, respectively<sup>1</sup>. The data were corrected for these inefficiencies in the analysis.

The two HPGe detectors used are commercial Extended Range (XtRa) coaxial germanium detectors, produced by CANBERRA [39]. Their nominal energy resolution is  $\approx 2$  keV at 1.3 MeV. These detectors are manufactured from cylindrical germanium crystals with radii of 3.5 cm, lengths of  $\approx 7$  cm and central bore holes with a length of 4.5 cm. The crystals are housed in cylindrical vacuum chambers made of aluminum. The detectors are in thermal contact with copper cooling fingers which extend beyond the lead castle to the electrical cooling units, see Figs. 3(b) and 5. Having electro-cooled germanium detectors makes MINIDEX an almost maintenance-free setup.

---

<sup>1</sup>These efficiencies were unexpectedly low. They cannot be explained by the geometrical effects due to the embedding of the PMTs. The PMT sidewalls were probably less sensitive than expected. A detailed investigation revealed that the PMTs were not properly optically coupled. The panels were replaced by Saint-Gobain and exchanged for conventional panels with external PMTs after run I.



#### 2.4. DAQ and Electronics

The DAQ system employed for MINIDEX is a 16-channel VME digitizer card, SIS3316-DT, produced by Struck Innovative Systems [40]. Each channel can be used independently from the others with a 250 MHz sampling rate. All channels are equipped with a 14-bit resolution ADC and run in double bank mode to avoid dead time. The time information is distributed to the channels via an internal clock.

All detector signals from MINIDEX are recorded independently without a shared trigger. Data are written to and stored in a server (sys-Gen/Supermicro SYS-5018D-MTF [41]) which is placed directly next to the DAQ on the lower shelf of the supporting table.

A two-channel HV power supply (iseg NHQ 206L) provides the high voltage for the HPGe detectors. Low voltage supplies support the preamplifiers of the germanium detectors and the scintillator panels. The whole system is being controlled remotely through a router, which provides access to every single device. To prevent damage to the germanium detectors from power cuts and to generally protect the system from noise due to the power line, MINIDEX is operated behind an uninterruptible power supply (Online XSR3000 PSU).

#### 2.5. Online Monitoring and Detector Performance

The MINIDEX apparatus is continuously monitored during operation. The energy spectra of the scintillators and the HPGe detectors are recorded and the data quality is constantly evaluated through the energy resolution of both HPGe detectors at 1460 keV ( $^{40}\text{K}$  line). Also recorded are the temperature of the water and its level inside the tank.

Figure 6 demonstrates the stability of the energy resolution of 2.2 keV at 1460 keV for the sum of the energy spectra of the two germanium detectors. Each point represents approximately two hours of data taking.

The temperature of the water was measured with a PT100 [42] temperature sensor placed inside the water tank. To measure the water level inside the tank, MINIDEX was equipped with a liquid-level sensor probe produced by Vegetronix [43]. The stability of both temperature and water level is demonstrated in Fig. 7. They vary only very little and the change in level is compatible with the expansion of the water due to temperature shifts. Thus, the mass of the water was constant; there were no leaks over the whole data taking period.

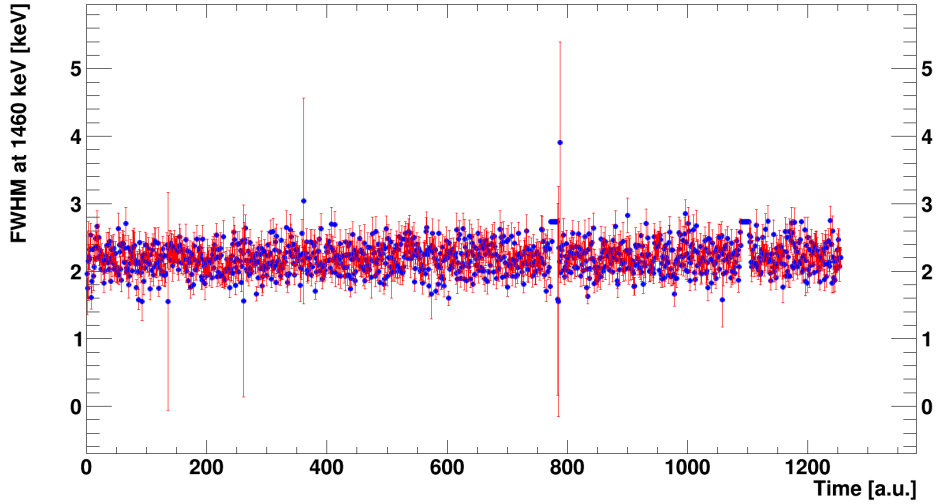


Figure 6: The energy resolution at 1460 keV of the sum of the spectra of the two germanium detectors vs. time. Each point corresponds to approximately two hours of data taking. All data collected between the beginning of MINIDEX run I and November, 25, 2015 are included. From [35].

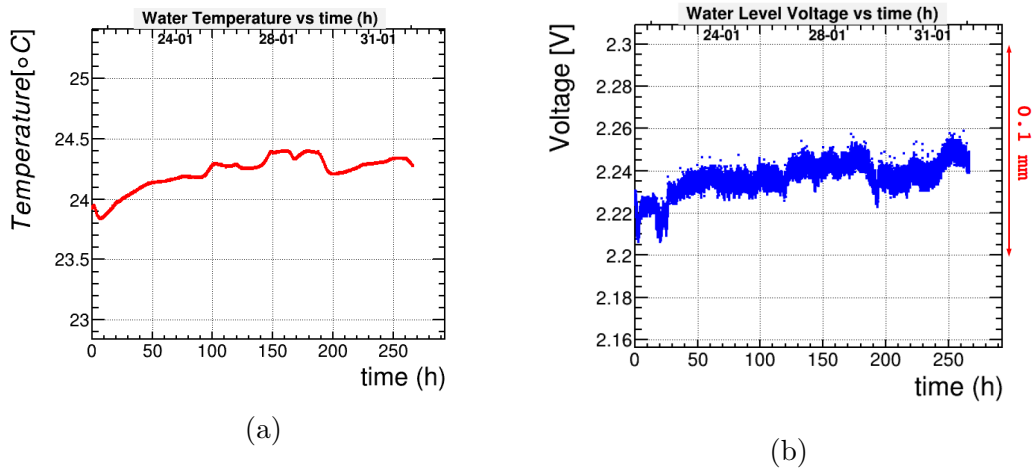


Figure 7: (a) Water temperature vs. time. (b) Water level vs. time; the signal is a voltage – a difference of 0.1 V corresponds to a change in water-level of  $100\ \mu\text{m}$ . Both adapted from [35].

### 3. Run I

Run I started on July 15, 2015, and the setup was operated in a stable configuration until January 19, 2016. The data taken until November 25, 2015 were included in the first analysis. They represent a run-time of  $9.8 \times 10^6$  s (114.4 days). This relates to an up-time of 86 % <sup>2</sup>.

#### 3.1. Offline trigger definition

The trigger for run I requires a muon passing through both the top and the bottom scintillator panels. Such muons are identified through signals in both panels within a time window to be determined. The signals from the top and bottom scintillators are recorded independently at times denoted  $T_{\text{top}}$  and  $T_{\text{bot}}$ , respectively. The distribution of the time difference  $T_{\text{top}} - T_{\text{bot}}$  is shown in Fig. 8. A very significant peak characterises the coincidences associated with the passage of muons. The width of the peak is related to time jitter. The trigger window chosen was  $[-40; +20]$  ns. For each triggered event,  $T_{\text{top}}$  was taken as the time of the passage of the muon,  $T_{\text{trig}}$ . No cut on the light observed in each panel was applied <sup>3</sup>.

Approximately  $10^8$  triggers were identified, corresponding to a trigger rate of  $\approx 10$  Hz. The individual total count rates of the scintillator panels were  $R_{\text{top}} = 49.3$  Hz and  $R_{\text{bot}} = 46.8$  Hz, respectively. Given the width of the coincidence window of  $\Delta T_{\text{coinc}} = 60$  ns, the corresponding accidental trigger rate of  $\approx 3 \times 10^{-4}$  Hz only produces a negligible contamination of the triggered events. Outside the trigger window, an excess of events with negative  $T_{\text{top}} - T_{\text{bot}}$  was observed. This is due to muons only passing through the top scintillator and secondary particles depositing energy in the bottom scintillator. For muons only passing through the bottom scintillator, it is less likely that secondary particles reach the top scintillator.

#### 3.2. Definition of signal window

The data recorded for the two HPGe detectors are divided into two time windows after each trigger:

- *INSIDE*: events recorded within a time window  $\Delta T_{\text{win}}$ ;
- *OUTSIDE*: events recorded between the end of  $\Delta T_{\text{win}}$  and the arrival of the next trigger.

---

<sup>2</sup>The down-time was caused by the infant mortality of HV supplies for the scintillators.

<sup>3</sup>As the spectra of the panels did not show a good separation between single hits and coincidences, this was unavoidable.

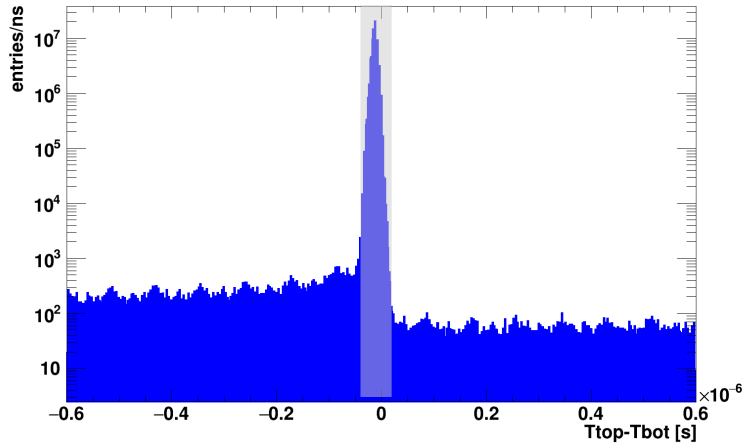


Figure 8: Distribution of the time difference  $T_{\text{top}} - T_{\text{bot}}$ . The value of a given  $T_{\text{top}}$  is compared to the previous and all following  $T_{\text{bot}}$  until a new  $T_{\text{top}}$  is recorded. The lightly shaded area around the pronounced peak corresponds to the trigger window. From [35].

The value of  $\Delta T_{\text{win}}$  is not fixed, i.e. the analysis is performed for multiple  $\Delta T_{\text{win}}$  to study the time evolution of the signal. Simulations performed for the design studies predicted that the time distribution of the muon-induced 2.2 MeV gammas seen by the germanium detectors would not extend significantly beyond 1 ms after the occurrence of a trigger. Thus, the average time between triggers of  $\approx 100$  ms is large enough to not affect the full collection of the signal.

With large enough  $\Delta T_{\text{win}}$ , the inside window fully contains the signal plus background while the corresponding outside window only contains events related to background. Thus, the background is measured in parallel to the signal. This procedure is illustrated in Fig. 9.

### 3.3. The germanium detector signal

The calibrated spectra of the germanium detectors were summed up for the inside and outside windows. Figure 10 shows the result for  $\Delta T_{\text{win}} = 4$  ms. Also shown in Fig. 10 are fits with a Gaussian plus a first order polynomial. The resolution of the 2.2 MeV peak is 2.8 keV FWHM. The contribution of neutron induced 2.2 MeV gammas is measured over a much larger time for the background than for the signal and thus, to a much higher precision. This is important for background subtraction.

The numbers of neutron-induced events,  $N_{\text{peak}}^{\text{inside}}$  and  $N_{\text{peak}}^{\text{outside}}$ , were

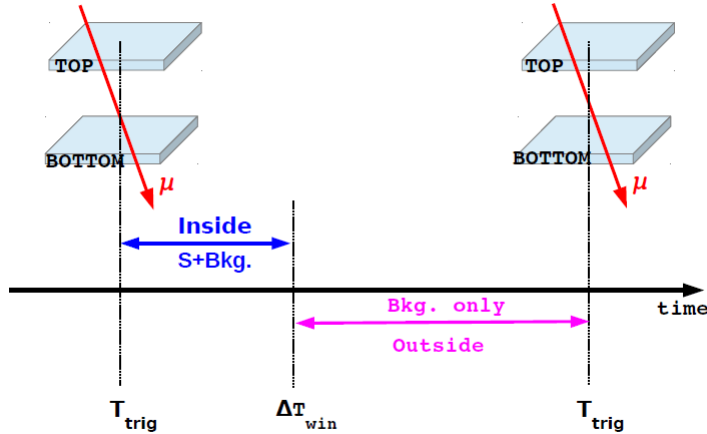


Figure 9: Sketch illustrating the analysis strategy adopted for MINIDEX run I. When  $\Delta T_{win}$  is big enough, the outside window contains only background (Bkg.) events. The inside window contains also the full signal(S). From [35].

evaluated from fits as shown in Fig 10. To evaluate the systematic uncertainty on the result of the extraction, a method based on side-bands around a region of interest of  $2.223 \text{ MeV} \pm 5 \text{ keV}$  was used [35]. Any difference between the methods was taken as a symmetric systematic uncertainty and added in quadrature to the statistical uncertainty. The systematic uncertainties are in general much smaller than the statistical uncertainties. They are only significant for very small  $\Delta T_{win}$ . Unless otherwise stated, total uncertainties are quoted.

#### 3.4. Evaluation of signal and background rates

The signal is determined through the rate of 2.2 MeV gammas recorded in the predefined time window after a muon trigger. The effective run-times accumulated in the signal window,  $ET_{inside}$ , and the background window,  $ET_{outside}$ , are defined as

$$ET_{inside} = N_{trig} \cdot \Delta T_{win} , \quad (1)$$

$$ET_{outside} = RT - ET_{inside} , \quad (2)$$

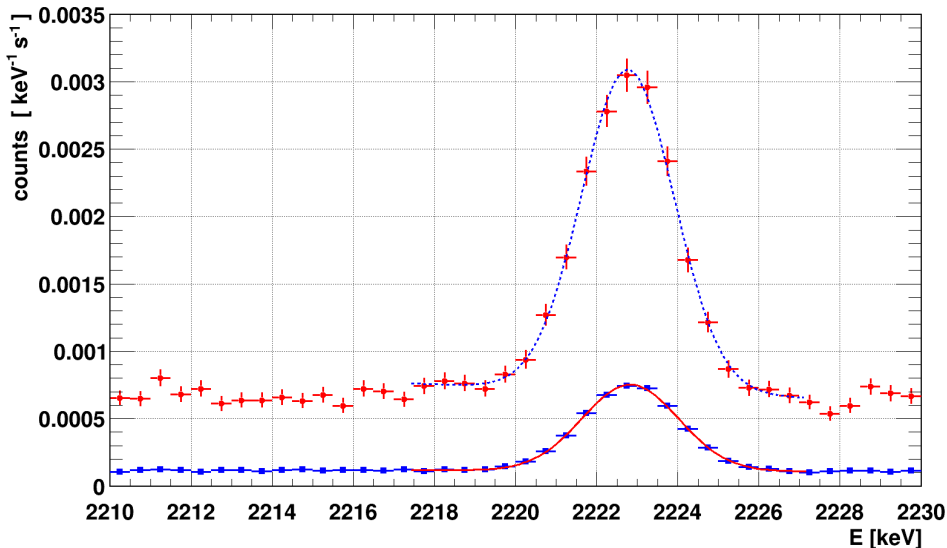


Figure 10: Summed time-normalised spectra of the two germanium detectors for inside (circles) and outside (squares) the  $\Delta T_{win} = 4$  ms window for the complete run-time. Both spectra were fit with a Gaussian plus a first order polynomial. The fit results are shown as a dotted (solid) line for the data inside (outside) the time window. The error bars represent the statistical uncertainties. For the outside spectrum, the statistical uncertainties are smaller than the size of the symbols.

where  $N_{trig}$  is the number of triggers<sup>4</sup> and RT the total run-time of the measurement.

The effective rates for signal plus background,  $\Gamma_{S+B}$ , and background,  $\Gamma_B$ , are defined as

$$\Gamma_{S+B} = N_{peak}^{inside} / ET_{inside} , \quad (3)$$

$$\Gamma_B = N_{peak}^{outside} / ET_{outside} . \quad (4)$$

The background rate,  $\Gamma_B$ , was evaluated for 39 values of  $\Delta T_{win}$ , see Fig. 11. The increase per step in  $\Delta T_{win}$  is  $10 \mu s$  up to  $200 \mu s$  and then the step size gradually gets larger. The background rate is expected to be time independent. For values of  $\Delta T_{win} < 1$  ms, a significant number of signal events

---

<sup>4</sup>Due to the inefficiency of the scintillators, some muons were not triggered and thus the resulting neutrons were not recorded as signal. This was corrected for by adjusting the number of triggers appropriately [35].

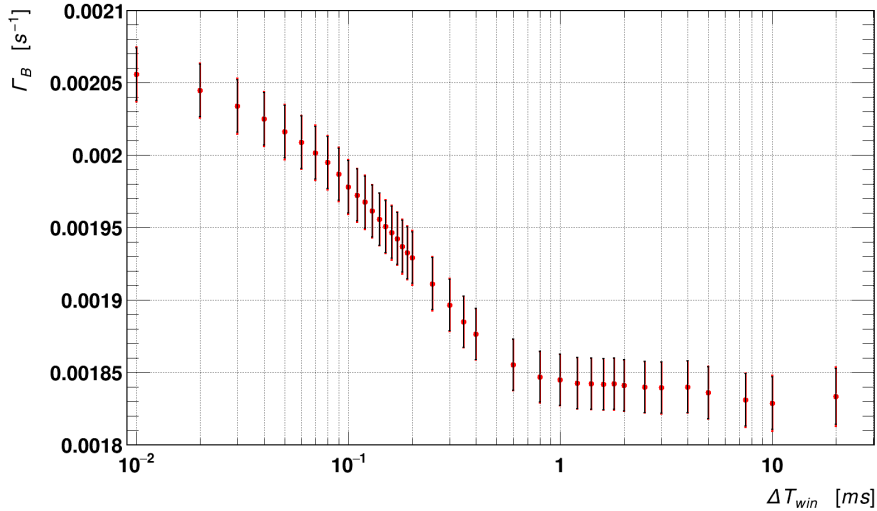


Figure 11: The effective rate,  $\Gamma_B$ , of events observed in the outside window. The inner error bars represent the statistical uncertainties, the outer bars represent the statistical and the systematic uncertainties added in quadrature. The statistical uncertainties dominate such that the outer error bars are almost invisible. The entries are highly correlated as the events for each window also contain the events in the smaller time windows.

are “leaking” into the background window. As expected, the rate flattens out at  $\Delta T_{win}$  values of around 1 ms. To determine the overall background rate,  $R_B$ , safely,  $\Delta T_{win}$  should be larger than 1 ms. A value of  $\Delta T_{win} = 4$  ms was chosen and  $R_B$  determined to be  $R_B = (1.84 \pm 0.02) \times 10^{-3}$  Hz. The effective signal rate,  $R_S$ , for all predefined signal windows was calculated as

$$R_S = \Gamma_{S+B} - R_B \quad . \quad (5)$$

### 3.5. Time evolution of the signal

Figure 12 shows the time evolution of the signal,  $N_{peak}^{inside}$ , accumulated in the 2.2 MeV peak in the gamma spectrum with growing  $\Delta T_{win}$  on a linear time scale. The values of  $N_{peak}^{inside}$  are correlated, since any  $\Delta T_{win}$  window contains all the events already recorded in the smaller time windows. The linear fit to the histogram for  $\Delta T_{win} \geq 2$  ms confirms a flat background rate. The intercept with the  $y$ -axis provides the total number of 2.2 MeV gammas that can be attributed to the signal.

The time evolution of the background-subtracted signal rate,  $R_S$ , is shown in Fig. 13 on the exponential time scale also used for the visualisation of the

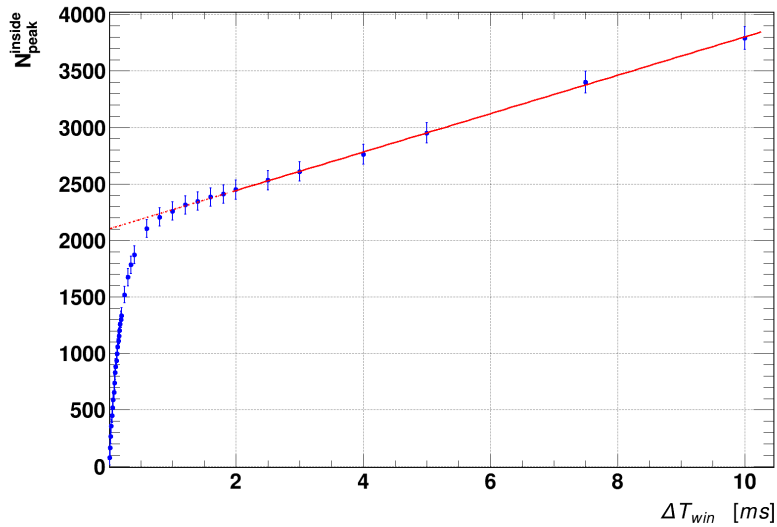


Figure 12: Number of events,  $N_{peak}^{inside}$ , accumulated vs.  $\Delta T_{win}$ . A linear fit, represented by a solid line, was performed for  $\Delta T_{win} \geq 2$  ms. The extrapolation to  $\Delta T_{win} = 0$  is shown as a dotted line. Error bars represent the uncertainties of the fit to the 2.2 MeV peak in the gamma spectra.

background rate in Fig. 11. The effective rates are the highest for  $\Delta T_{win}$  between  $20 \mu s$  and  $100 \mu s$ . The rates then drop, which is equivalent to a decreasing number of signal events added per unit time. Beyond 1 ms, no new signal events are recorded and thus the effective rate drops due to the larger windows considered. Clearly,  $\Delta T_{win}$  up to 1 ms can be chosen for all studies of the signal. The signal-to-background ratios,  $\rho_{S/B} = R_S/R_B$ , for such windows are shown to be above 15 in Fig. 14. For  $\Delta T_{win}$  between  $20 \mu s$  and  $100 \mu s$ ,  $\rho_{S/B}$  reaches values of up to 60.



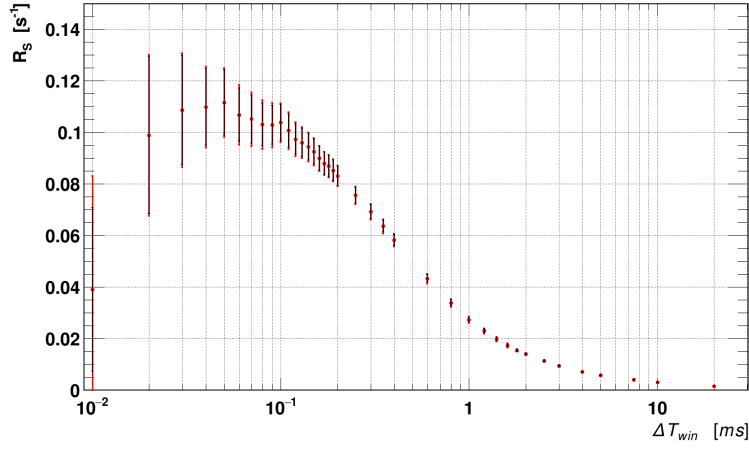


Figure 13: Effective signal rate,  $R_S$ , vs.  $\Delta T_{win}$ . The inner error bars represent the statistical uncertainties, the outer bars represent the statistical and the systematic uncertainties added in quadrature. Adapted from [35].

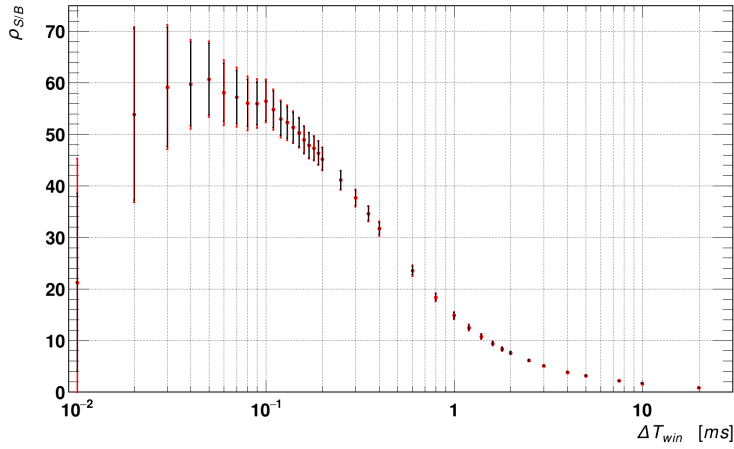


Figure 14: Signal-to-background ratio,  $\rho_{S/B}$ , vs.  $\Delta T_{win}$ . The inner error bars represent the statistical uncertainties, the outer bars represent the statistical and the systematic uncertainties added in quadrature. Adapted from [35].

#### 4. Comparison of Monte Carlo to data

The run I trigger configuration does not facilitate to distinguish between events in the side-wall and elsewhere in the apparatus. The resulting definition of signal and background for run I makes a direct physics interpretation

of the data in terms of the neutron production rate in lead difficult. However, the data can be compared to Monte Carlo predictions.

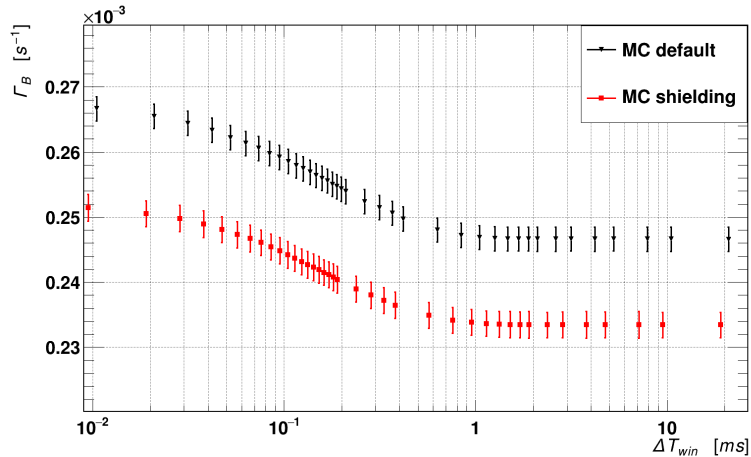


Figure 15: Effective MC rate,  $\Gamma_B^{MC}$ , see Eq. 4, vs.  $\Delta T_{win}$  for the physics lists default and shielding.

The simulations were performed within the Monte Carlo (MC) framework MaGe [44], jointly developed by the GERDA [45] and MAJORANA [21] collaborations. Two different “physics lists” were used:

- **default** as recommended by the MaGe developers;
- **shielding** as recommended by the GEANT4 collaboration [46].

These two physics lists differ mainly on the production of neutrons in the primary interaction of the muon and in secondary hadronic interactions. They are basically identical on neutron transport.

A simplified version [35] of the overburden of the TSUL, together with a detailed description of the MINIDEX run I apparatus were implemented in GEANT4 (version 9.6.4 [47]). The cosmic muon [48] and neutron [49] spectra were used as input; both, muons and neutrons were tracked into the experimental volume, where their interactions were simulated.

The energy resolution of the HPGe detectors was taken into account by smearing all energies according to a Gaussian distribution with a constant standard deviation of 1.6 keV. This value corresponds to a FWHM of  $\approx 2.8$  keV as measured for the peak at 2.2 MeV. Since all the comparisons of MC to data only refer to the region around 2.2 MeV, the simplification of a constant resolution is justified.

The background components due to cosmic muons and neutrons were simulated together with the signal. The background contribution from cosmic neutrons was found to be around one order of magnitude smaller than from non-triggering cosmic muons [35].

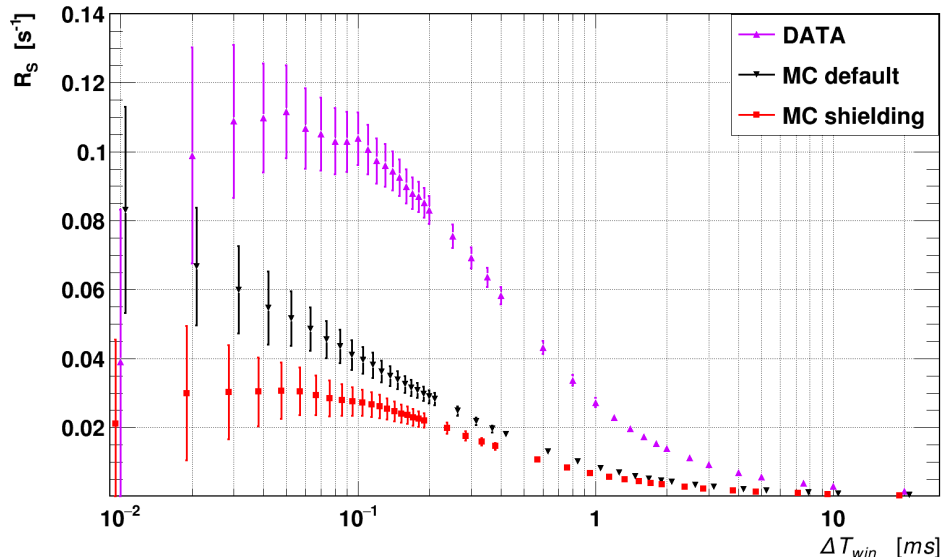


Figure 16: Comparison of the MC predictions from the two physics lists for  $R_S$  to data. The points are horizontally displaced for better visibility. The error bars represent the total uncertainties, which are highly correlated.

The analysis of the MC data was performed exactly as for data with equivalent definitions for  $\Gamma_B^{MC}$ ,  $R_S^{MC}$ . Figure 15 shows the time evolution of the rate  $\Gamma_B^{MC}$  vs.  $\Delta T_{win}$ . The background contribution has already flattened out at 1 ms where the influence of the signal ends. This is slightly earlier than observed for the data, see Fig. 11. The prediction for  $\Gamma_B^{MC}$  from the default list is about 5% higher than from the shielding list for  $\Delta T_{win} > 1$  ms.

The component due to natural radioactivity was not included in the simulation. This creates a large discrepancy in the absolute background rate between the MC and data. The background measured with  $\Delta T_{win} = 4$  ms is more than a factor of seven higher in the data than predicted for the cosmogenic contribution alone. This shows, that the background due to natural radioactivity is dominating in the data.

The background-subtracted signal rate  $R_S$ , see Eq. 5, allows a direct comparison of Monte Carlo predictions to data. This is shown in Fig. 16. Both physics lists predict significantly smaller signals than observed. Table 1 lists

$R_S$  for  $\Delta T_{win} = 4$  ms as measured and predicted by the two MC versions. The data exceed the predictions from the MaGe default (GEANT shielding) Monte Carlo by a factor of 3.3 (4.1). The MaGe default list predicts a strong prompt signal, not observed in the data while the GEANT shielding list qualitatively describes the time evolution reasonably well.

Effective Signal Rate $R_S$ for	
Data	$(7.0 \pm 0.2) 10^{-3}$ Hz
GEANT with “MaGe default” list	$(2.1 \pm 0.1) 10^{-3}$ Hz
GEANT with “GEANT shielding” list	$(1.7 \pm 0.1) 10^{-3}$ Hz

Table 1: Effective signal rate,  $R_S$ , for  $\Delta T_{win} = 4$  ms for data and the two MCs.

Another approach is to compare the MC to data before background subtraction. The muon-induced components of the MC predictions are separated out by fitting the MC predictions to the data for each  $\Delta T_{win}$ :

$$(\Gamma_{S+B})_i = A_i \cdot [ (\Gamma_{tr-\mu}^{inside})_i^{MC} + \Gamma_{ntr-\mu}^{MC} ] + B_i \cdot \Gamma_{neutrons}^{MC} \quad (6)$$

$$R_B = A_i \cdot \Gamma_{ntr-\mu}^{MC} + B_i \cdot \Gamma_{neutrons}^{MC} \quad (7)$$

where:

- the index  $i$  is the ascending index for the different  $\Delta T_{win}$ ;
- $A_i$  and  $B_i$  are the fit parameters for window  $i$ .  $A_i$  represent the factors by which the muon-induced components are scaled to fit the data.  $B_i$  represent the factors by which the background due to cosmic neutrons is scaled to account for the non-simulated background due to natural radioactivity;
- $(\Gamma_{S+B})_i$  is the measured  $\Gamma_{S+B}$  for window  $i$ ;
- $R_B$  is the measured background rate;
- $(\Gamma_{tr-\mu}^{inside})_i^{MC}$  is the simulated effective signal rate due to triggered muons for window  $i$ ;
- $\Gamma_{ntr-\mu}^{MC}$  is the simulated background rate due to non-triggered muons;
- $\Gamma_{neutrons}^{MC}$  is the simulated background rate due to cosmic neutrons.

It is possible to scale up the background due to cosmic neutrons to include the background due to natural radioactivity, because both background contributions are constant in time and only the 2.2 MeV gamma peak is considered. The results of the fits are depicted in Fig. 17 and listed in Table 2.

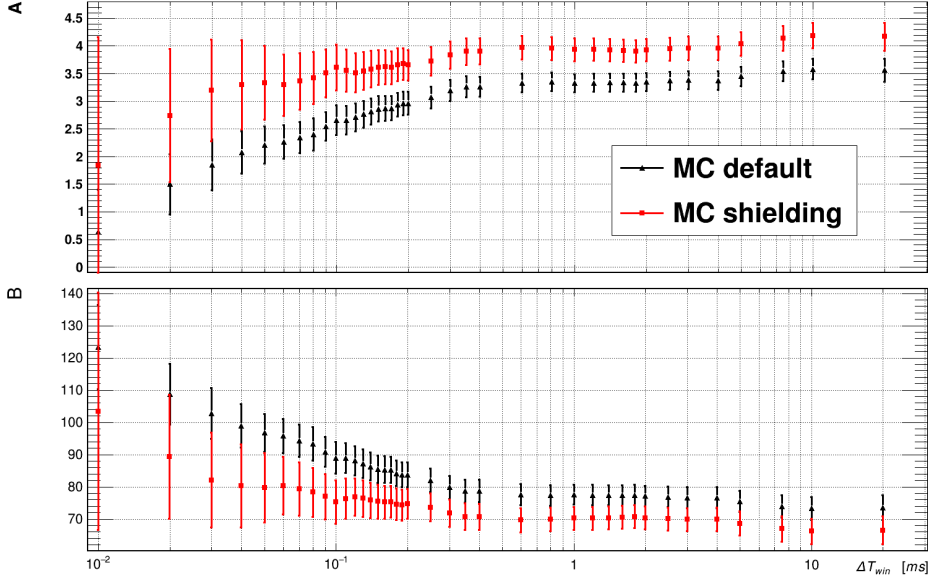


Figure 17: Scale parameters  $A_i$  and  $B_i$  vs.  $\Delta T_{win}$  as obtained for the two different physics lists. The error bars represent statistical uncertainties only. They are highly correlated as each time window contains all events recorded already in smaller time windows.

If the time evolution of the signal was perfectly described by the simulation, the parameters  $A_i$  and  $B_i$  would be constant for all  $i$ . However, as already seen in Fig. 16, this is not the case. The values of  $B_i$  are actually quite stable over most of the range. At very small  $\Delta T_{win}$ , where the statistical uncertainty is large, the  $B_i$  increase as the procedure tries to compensate for the lacking signal strengths in the MCs. As the shielding list describes the time evolution of the signal reasonably well, the parameters  $A_i$  vary not so much. For the MaGe default physics list, the value of  $A_1$  actually drops below one. This confirms that this MC predicts a fast component of the signal not present in the data.

$\Delta T_{win}$ [ms]	$A_i$		$B_i$	
	MaGe default	GEANT shielding	MaGe default	GEANT shielding
0.01	0.64 ± 0.77	1.84 ± 2.33	123 ± 13	104 ± 37
0.02	1.50 ± 0.55	2.74 ± 1.21	109 ± 9	89 ± 19
0.03	1.85 ± 0.46	3.19 ± 0.92	103 ± 8	82 ± 15
0.04	2.08 ± 0.39	3.30 ± 0.81	99 ± 7	80 ± 13
0.05	2.20 ± 0.33	3.34 ± 0.67	97 ± 6	80 ± 11
0.06	2.27 ± 0.30	3.30 ± 0.56	96 ± 5	80 ± 9
0.07	2.35 ± 0.28	3.36 ± 0.51	94 ± 5	79 ± 8
0.08	2.40 ± 0.29	3.43 ± 0.47	93 ± 5	78 ± 8
0.09	2.55 ± 0.26	3.51 ± 0.43	91 ± 5	77 ± 7
0.10	2.66 ± 0.27	3.61 ± 0.42	89 ± 5	75 ± 7
0.11	2.66 ± 0.26	3.55 ± 0.38	89 ± 5	76 ± 6
0.12	2.71 ± 0.25	3.52 ± 0.36	88 ± 5	77 ± 6
0.13	2.77 ± 0.24	3.55 ± 0.34	87 ± 4	76 ± 6
0.14	2.82 ± 0.24	3.58 ± 0.33	86 ± 4	76 ± 5
0.15	2.87 ± 0.23	3.61 ± 0.32	86 ± 4	75 ± 5
0.16	2.87 ± 0.23	3.62 ± 0.31	85 ± 4	75 ± 5
0.17	2.88 ± 0.22	3.61 ± 0.30	85 ± 4	75 ± 5
0.18	2.94 ± 0.22	3.66 ± 0.30	84 ± 4	75 ± 5
0.19	2.97 ± 0.21	3.68 ± 0.29	84 ± 4	74 ± 5
0.20	2.96 ± 0.21	3.65 ± 0.28	84 ± 4	75 ± 5
0.25	3.07 ± 0.20	3.72 ± 0.26	82 ± 4	74 ± 4
0.30	3.20 ± 0.19	3.83 ± 0.25	80 ± 4	72 ± 4
0.35	3.26 ± 0.19	3.90 ± 0.24	79 ± 4	71 ± 4
0.40	3.26 ± 0.18	3.91 ± 0.23	79 ± 3	71 ± 4
0.60	3.33 ± 0.17	3.97 ± 0.22	78 ± 3	70 ± 4
0.80	3.34 ± 0.17	3.96 ± 0.21	77 ± 3	70 ± 4
1.00	3.33 ± 0.16	3.94 ± 0.21	78 ± 3	70 ± 4
1.20	3.34 ± 0.16	3.94 ± 0.21	78 ± 3	70 ± 4
1.40	3.34 ± 0.16	3.93 ± 0.21	77 ± 3	70 ± 4
1.60	3.34 ± 0.16	3.91 ± 0.20	77 ± 3	71 ± 4
1.80	3.34 ± 0.16	3.91 ± 0.20	78 ± 3	71 ± 4
2.00	3.35 ± 0.16	3.93 ± 0.21	77 ± 3	70 ± 4
2.50	3.37 ± 0.17	3.95 ± 0.21	77 ± 3	70 ± 4
3.00	3.38 ± 0.17	3.96 ± 0.21	77 ± 3	70 ± 4
4.00	3.38 ± 0.17	3.96 ± 0.21	77 ± 3	70 ± 4
5.00	3.45 ± 0.17	4.04 ± 0.21	76 ± 3	69 ± 4
7.50	3.54 ± 0.18	4.14 ± 0.23	74 ± 3	67 ± 4
10.00	3.58 ± 0.19	4.19 ± 0.23	73 ± 4	66 ± 4
20.00	3.56 ± 0.21	4.17 ± 0.25	74 ± 4	67 ± 4

Table 2: Values of the scale factors  $A_i$  and  $B_i$  for each  $\Delta T_{win}$  for both MC predictions. Uncertainties are statistical only.

## 5. Summary and Outlook

A new experiment to measure the production of neutrons by cosmic muons, MINIDEX, was introduced. It is a compact apparatus, easy to move to different locations, almost maintenance free and operated remotely. Neutrons are detected after thermalisation through 2.2 MeV gammas emitted after their capture by the hydrogen in water. Thus, MINIDEX measures neutrons without an energy threshold. The signal and the background are measured simultaneously, allowing the extraction of the signal and its time evolution without major assumptions or Monte Carlo simulations.

The results of the first run of MINIDEX with lead as the target material and at a depth of about 16 meter water equivalent were presented. A clear signal was observed with signal-to-background ratios above 15 for the complete development of the signal over one millisecond. The results were compared to GEANT 4 based Monte Carlo simulations using the so called “MaGe default” and “GEANT shielding” physics lists. Both lists led to predictions that underestimate the integrated signal strength significantly. The data show an overall production of muon-induced 2.2 MeV gammas a factor of 3.3 (4.1) higher than predicted using the MaGe default (GEANT 4 shielding) list. While the shielding list does not describe the overall signal strength as well as the MaGe default list it qualitatively describes the time evolution better. In particular, the MaGe default list predicts a prompt signal component not observed in the data.

During its first data taking period, MINIDEX ran with a very simple muon trigger. In January 2016, the setup was upgraded to allow for the identification of different event topologies. Especially, muons can be identified that pass vertically and only through the selected high-Z material. Different event topologies should also provide some handle to disentangle the primary neutron production rate from the influence of neutron transport.

At the end of 2016, a switch to copper as the target material is foreseen. The data is expected to be available as input to the design phase of the next-generation large-scale low-background experiments currently envisioned, where lead and copper are discussed as shielding materials. During the following years, MINIDEX will explore the neutron production due to cosmic muons in a variety of high-Z materials. In addition, the dependence on the muon energy can be probed by moving MINIDEX to different depths.

## 6. Acknowledgments

We would like to thank the technical department of the Max-Planck-Institut für Physik for their strong support. We would also like to thank the

Universität Tübingen for the space in TSUL, especially Peter Grabmaier and Igor Usherov for their hospitality and help.

## Bibliography:

### References

- [1] O.C. Allkofer and R.D. Andresen, Nucl. Phys. B 8, 402 (1968)
- [2] M. Aglietta et al., Nuovo Cimento Soc. Ital. Fis., C 12, 467 (1989)
- [3] M. Aglietta et al., in Proceedings of the 26th International Cosmic Ray Conference, Salt Lake City, 1999, edited by D. Kieda, M. Salamon, and B. Dingus, Vol. 2, p. 44, hep-ex/9905047
- [4] R. Hertenberger, M. Chen, and B.L. Dougherty, Phys. Rev. C 52, 3449 (1995)
- [5] F. Boehm et al., *Neutron production by cosmic-ray muons at shallow depth*, Phys. Rev. D 62, 092005 (2000)
- [6] J. Rapp, Ph.D. thesis, University of Karlsruhe, 1996
- [7] T. Langford et al., *Fast neutron detection with a segmented spectrometer*, Nucl. Instrum. Meth. A 771 (2015), 78-87
- [8] J. Delorme et al., Phys. Rev. C 52, 2222 (1995)
- [9] O.G. Ryazhskaya and G.T. Zatsepin, Izv. Akad. Nauk SSSR, Ser. Fiz. 29, 1946 (1965); in Proceedings of the IX International Conference on Cosmic Rays, London, 1965, Vol. 21, p.987
- [10] J.C. Barton, in Proceedings of the 19th International Conference on Cosmic Rays, La Jolla, 1985, edited by F. C. Jones Physical Society, London, 1985), p. 98.
- [11] D.H. Perkins, *Calculation of neutron background in Soudan 1990*.
- [12] D.-M. Mei and A. Hime, *Muon-Induced Background Study for Underground Laboratories*, Phys. Rev. D 73, (2006) 053004
- [13] H. M. Araújo et al., Nucl. Instrum. Meth. A 545 (2005), 398.
- [14] J. A. Formaggio and C. J. Martoff, *Backgrounds to Sensitive Experiments Underground*, Annu. Rev. Nucl. Part. Sci. 54, 361 (2004)



- [15] H. Wulandari et al., *Neutron Background Studies for the CRESST Dark Matter Experiment*, hep-ex/0401032
- [16] A. Empl et al, *A Fluka study of underground cosmogenic neutron production*, JCAP08 (2014) 064
- [17] A. Gando et al, KamLAND-Zen Collaboration, Phys. Rev. Lett. 110, 062502 (2013)
- [18] J. B. Albert et al., EXO Collaboration, Nature 510, (2014) 229
- [19] M. Agostini et al., GERDA Collaboration, *Results on Neutrinoless Double- $\beta$  Decay of  $^{76}\text{Ge}$  from Phase I of the GERDA Experiment*, Phys. Rev. Lett 111 (2013) 122503
- [20] M. Agostini, *First results from GERDA Phase II*, (2016), Presentation at NEUTRINO2016, London, United Kingdom
- [21] The Majorana Collaboration, Phys. of Atom. Nucl. Vol. 67, Issue 11 , pp 2002-2010, DOI: 10.1134/1.1825519
- [22] The CDEX Collaboration, Front. Phys., 2013, 8(4):412-437
- [23] D.S. Akerib et al, CDMS Collab., *First Results from the Cryogenic Dark Matter Search in the Soudan Underground Laboratory*, Phys. Rev. Lett 93, 211301 (2004)
- [24] R. Brun et. al, *GEANT 3*, CERN DD/EE/84-1, 1987
- [25] Geant4 Collaboration, Nucl. Instrum. Meth. A 506 (2003), 250.
- [26] A. Fassò, A. Ferrari and P.R. Sala in: *Proceedings of MonteCarlo 2000 Conference*, (Lisbon, October 23-26, 2000), Ed. A. Kling, F. Barao, M. Nakagawa, L. Távora, P. Vaz (Springer-Verlag, Berlin, 2001).
- [27] V.A. Kudryavtsev, N.J. Spooner and J.E. McMillan, Nucl. Instrum. Meth. A 505 (2003)
- [28] Y.F. Wang et al., *Predicting neutron production from cosmic-ray muons*, Phys. Rev. D 62, 013012 (2000)
- [29] C. Zhang and D.-M. Mei, *Measuring Muon-Induced Neutrons with Liquid Scintillation Detector at Soudane Mine*, Phys. Rev. D 90, 122003
- [30] L. Reichhart et al., *Measurement and simulation of the muon-induced neutron yield in lead*, Astropart. Phys. 47 (2013) 67-76

- [31] M. G. Marino et al., *Validation of spallation neutron production and propagation within Geant4*, Nucl. Instrum. Meth. A 582 (2007), 611-620
- [32] A. Lindote et al., *Simulation of neutrons produced by high-energy muons underground*, Astropart. Phys. 31 (2009), 366-375
- [33] M. Horn, *Simulations of the muon-induced neutron background of the EDELWEISS-II experiment for Dark Matter search*, Ph.D. Thesis, Institut für Experimentelle Kernphysik, Karlsruhe, 2007
- [34] H. Kluck, *Measurement of the cosmic-induced neutron yield at the Modane underground laboratory*, Ph.D. Thesis, Institut für Experimentelle Kernphysik, Karlsruhe, 2013
- [35] M. Palermo, *The Muon-Induced Neutron Indirect Detection EXperiment, MINIDEX*, Ph.D. Thesis, Max-Planck Institute for Physics, Munich, 2016
- [36] Peter Grabmaier, Universität Tübingen, private communication
- [37] <http://www.crystals.saint-gobain.com>, Retrieved on 26-01-2016
- [38] <http://www.et-enterprises.com/>, Retrieved on 26-01-2016
- [39] <http://www.canberra.com/products/detectors/germanium-detectors.asp>, Retrieved on 27-01-2016
- [40] <http://www.struck.de/sis3316.html>, Retrieved on 27-01-2016
- [41] <http://www.supermicro.com/products/system/1u/5018/SYS-5018D-MTF.cfm>, Retrieved on 27-01-2016
- [42] [https://en.wikipedia.org/wiki/Resistance\\_thermometer](https://en.wikipedia.org/wiki/Resistance_thermometer), Retrieved on 01-02-2016
- [43] <http://www.vegetronix.com/Products/AquaPlumb/>, Retrieved on 01-02-2016
- [44] M. Bauer et al., *MaGe: a Monte Carlo framework for the Gerda and Majorana double beta decay experiments*, J. Phys. Conf. Ser. 39, (2006) 362
- [45] The GERDA Collaboration, Eur. Phys. J. C 73 (2013) 2330 DOI: 10.1140/epjc/s10052-013-2330-0

- [46] [http://geant4.cern.ch/support/proc\\_mod\\_catalog/physics\\_lists/useCases.shtml](http://geant4.cern.ch/support/proc_mod_catalog/physics_lists/useCases.shtml),  
Retreived on 17-02-2016
- [47] Geant4 9.6 Release Notes, <http://geant4.cern.ch/support/ReleaseNotes4.9.6.html>,  
Retreived 03/11/2015
- [48] M. Duranti, *Measurement Of The Atmospheric Muon Flux On Ground With The AMS-02 Detector*, PhD Thesis, 2011
- [49] Gordon et al, *Measurement of the Flux and Energy Spectrum of Cosmic-Ray Induced Neutrons on the Ground*,IEEE Transactions on Nucl. Sci.,  
Vol. 51, No. 6, December 2004